A dynamic model-based preparation of uniformly-^{13}C-labeled internal standards facilitates quantitative metabolomics analysis of Penicillium chrysogenum

Wang, Guan; Chu, Ju; Zhuang, Yingping; van Gulik, Walter; Noorman, Henk

DOI
10.1016/j.jbiotec.2019.04.021

Publication date
2019

Document Version
Final published version

Published in
Journal of Biotechnology

Journal of Biotechnology 299 (2019) 21–31

Contents lists available at ScienceDirect

Journal of Biotechnology

journal homepage: www.elsevier.com/locate/jbiotec

A dynamic model-based preparation of uniformly-^{13}C-labeled internal standards facilitates quantitative metabolomics analysis of *Penicillium chrysogenum*

Guan Wang[a,*], Ju Chu[a], Yingping Zhuang[a,*], Walter van Gulik[b], Henk Noorman[c,d]

[a] State Key Laboratory of Bioreactor Engineering, East China University of Science and Technology (ECUST), Shanghai, People's Republic of China
[b] Cell Systems Engineering, Department of Biotechnology, Delft University of Technology, Delft, the Netherlands
[c] DSM Biotechnology Center, Delft, the Netherlands
[d] Department of Biotechnology, Delft University of Technology, Delft, the Netherlands

ARTICLE INFO

Keywords:
Dynamic
Fed-batch model
Isotope dilution mass spectrometry (IDMS)
Perturbation
Metabolomics
Penicillium chrysogenum

ABSTRACT

Targeted, quantitative metabolomics can, in principle, provide precise information on intracellular metabolite levels, which can be applied to accurate modeling of intracellular processes required in systems biology and metabolic engineering. However, quantitative metabolite profiling is often hampered by biased mass spectrometry-based analyses caused by matrix effects, the degradation of metabolites and metabolite leakage during sample preparation, and unexpected variation in instrument responses. Isotope Dilution Mass Spectrometry (IDMS) has been proven as the most accurate method for high-throughput detection of intracellular metabolite concentrations, and the key has been the acquisition of the corresponding fully uniformly (U) -^{13}C-labeled metabolites to be measured. Here, we have prepared U-^{13}C-labeled cell extracts by cultivating *P. chrysogenum* in a fed-batch fermentation with fully U-^{13}C-labeled substrates. Towards this goal, a dynamic fed-batch model describing *P. chrysogenum* growth and penicillin production was used to simulate the fermentation process and design the fed-batch fermentation media. Further, a case study with extensive intracellular metabolomics data from glucose-limited cultivation of *Penicillium chrysogenum* under both single and repetitive glucose pulses was illustrated by using the IDMS methods with the prepared U-^{13}C-labeled cell extracts as internal standards. In conclusion, the IDMS method can be incorporated into well-established fast sampling and quenching protocols to obtain dynamic quantitative in vivo metabolome data at the timescales of (tens of) seconds and elucidate the underlying regulatory architecture. The case study revealed gross differences between single and repeated pulses, which suggests that single pulse studies have limited value for understanding of metabolic responses in large-scale bioreactors. Instead, intermittent feeding should be favored.

1. Introduction

It has recently been reasoned that the net rates of cellular metabolic reactions are strongly driven by substrate concentrations and metabolite concentrations, which collectively have more than twice as much physiological impact than enzymes alone (Canelas et al., 2010; Hackett et al., 2016). This is quite reasonable because protein-metabolite interactions, e.g., allosteric regulation or competitive inhibition, play an indispensable role in homeostasis and in fast adaptations to abrupt environmental changes (Nasution et al., 2006; Reznik et al., 2017; Taymaz-Nikerel et al., 2013). However, a major knowledge gap resides in the identification of the metabolites which are involved in such interactions (Chubukov et al., 2013; Gerosa and Sauer, 2011). To bridge this gap, dynamic metabolite concentrations, as response to a sudden metabolic perturbation, can be used to obtain in vivo kinetic properties of the pathway enzymes because they are the end products of the cellular regulatory processes, and the levels can be regarded as the ultimate response of biological systems to genetic or environmental changes (Fiehn, 2002). Furthermore, with accurate dynamic metabolomics data, highly predictive metabolic models can be established to understand, predict and optimize the properties and behaviors of the cell factory in a dynamic environment (Almquist et al., 2014; Deshmukh et al., 2015).

Nevertheless, monitoring metabolome changes is experimentally tedious and demanding, such that dynamic data on time scales from seconds to hours/days are extremely scarce (Link et al., 2015). To make

* Corresponding authors.
E-mail addresses: guanwang@ecust.edu.cn (G. Wang), ypzhuang@ecust.edu.cn (Y. Zhuang).

https://doi.org/10.1016/j.jbiotec.2019.04.021
Received 5 February 2019; Received in revised form 3 April 2019; Accepted 25 April 2019
Available online 29 April 2019
0168-1656/

the matters worse, achieving the absolute quantification of multiple metabolites is greatly hampered by ion enhancement or ion suppression in mass spectrometry (MS) analyses caused by matrix effects, the degradation of metabolites and metabolite leakage during sample preparation, and unexpected variation in instrument responses (Schatschneider et al., 2018). This biased metabolite level will lead to misinterpretation of functional information about the biochemical and physiological states of cells and cannot be applied to accurate modeling of intracellular processes required in systems biology and metabolic engineering. To address this problem, the Isotope-Dilution Mass Spectrometry (IDMS) method has been proven to be the most reliable technique because this approach can correct for most aspects of analytical biases (Mashego et al., 2004). The stable isotope dilution theory states that the relative signal intensity in a MS of two analytes that are chemically identical but of different stable isotope composition, distinguishable in a mass analyzer, are a true representation of the relative abundance of the two analytes in a sample (Mashego et al., 2004). Several research groups have used the IDMS method for the generation of accurate, quantitative MS-derived metabolite data (Bennett et al., 2008; Li et al., 2018; Patacq et al., 2018; Schatschneider et al., 2018; Seifar et al., 2009, 2008; Stafsnes et al., 2018; Vielhauer et al., 2011; Wu et al., 2005).

Penicillium chrysogenum is the most important cell factory for the production of β-lactam antibiotics, such as penicillin G, penicillin V and other derivatives (Ozcengiz and Demain, 2013). However, from a stochiometric point of view, the yields of these products are still low in current high-producing *Penicillium* strains (Prausse et al., 2016; van Gulik et al., 2001). Metabolic engineering and the optimization of bioreactor conditions are required for more efficient production. However, this requires fast and accurate physiological strain characterization. Towards this goal, combining mathematical models and experimental evidence renders a system-level understanding of metabolic behavior. Our research group has applied quantitative metabolomics studies of *Penicillium chrysogenum* to deliver information for computational metabolic modeling and reveal regulatory mechanisms in response to genetic or environmental perturbations (Tang et al., 2017; Wang et al., 2018a, b; Wang et al., 2019).

Here, we reported a model-based strategy to prepare U-^{13}C-labeled cell extracts as internal standards of *Penicillium chrysogenum* for quantitative metabolomics studies. A flowchart for preparation of uniformly ^{13}C labeled cell extracts and fast sampling, quenching and metabolite extraction for quantitative metabolomics of *P. chrysogenum* is provided (Fig. 1). Further, a case study with extensive dynamic intracellular metabolomics data from glucose-limited cultivation of *Penicillium chrysogenum* as response to both single and repetitive glucose pulses is illustrated by using the IDMS method with the prepared U-^{13}C-labeled cell extracts as internal standards.

2. Materials and methods

2.1. Part I. Preparation of U-^{13}C-labeled cell extracts

2.1.1. A dynamic fed-batch model for process simulation

The dynamic fed-batch model contains a) The previously published dynamic gene regulation model for *P. chrysogenum growth* and penicillin production (Eq. (1)); b) The Herbert-Pirt relation for substrate (Eq. (2)); c) Bioreactor mass balance (Eqs.3); d) Mass balances for substrate, biomass and penicillin (Eqs. (4)–(6)); e) Hyperbolic glucose uptake kinetics (Eq. (7)); f) Carbon and degree of reduction balances to obtain q_{O2} and q_{CO2} needed for the mass balance (Eqs. (8),(9)); g) The phenylacetic acid (PAA) balance (Eq.(10)).

$$\frac{dq_{PenG}}{dt} = \beta\mu\frac{1}{1+(C_S/K_P)^m} - (k_{dE}+\mu)q_{PenG} \quad (1)$$

$$\mu = Y_{SX}^{Max}\left(q_S - \frac{q_{PenG}}{Y_{SP}^{Max}} - m_S\right) \quad (2)$$

$$\frac{dM}{dt} = F_{in} + MW_{O2}q_{O2}MC_X - MW_{CO2}q_{CO2}MC_X \quad (3)$$

$$\frac{dC_sM}{dt} = F_{in}C_{S,in} - q_SMC_X \quad (4)$$

$$\frac{dC_XM}{dt} = \mu MC_X \quad (5)$$

$$\frac{dC_{PenG}M}{dt} = q_{PenG}MC_X \quad (6)$$

$$q_S = q_S^{Max}\frac{C_S}{K_S + C_S} \quad (7)$$

$$q_{O2} = 0.25(4q_S + 36q_{PAA} - 4.15\mu - 74q_{PenG}) \quad (8)$$

$$q_{CO2} = q_S - \mu - 16q_{PenG} + 8q_{PAA} \quad (9)$$

$$q_{PAA} = q_{PenG} \quad (10)$$

The flow rate: $0 < t < 12$ h, $F_{in} = 0$; $t > 12$ h, $F_{in} = \mu M$; Initial conditions: $M_0 = 0.3$ kg; $C_{S,0} = 0.806$ (Cmolglucose/kg broth); $C_X = 0.017$ (Cmol biomass/kg broth); $C_{PenG} = 0$ (mol penicillin/kg broth); $q_{PenG} = 0$ (mol penicillin/Cmol biomass/h). Parameters from Douma et al. (2010b); de Jonge et al. (2011) and van Gulik et al. (2001) used in the model can be found in Table 1. It should be noted that the glucose repression constant K_P was re-estimated based on the updated K_S by de Jonge et al. (2011) due to the improved glucose analysis method. The fed-batch fermentation process was simulated using Matlab 2018b.

2.1.2. Strains

A high-yielding *Penicillium chrysogenum* strain, DS 17690, was used. This strain was kindly donated by DSM Sinochem Pharmaceuticals (Delft, the Netherlands) as spores on rice grains; this strain has been extensively studied (Nasution et al., 2008; Wang et al., 2018a, b).

2.1.3. Medium

Batch medium (per kg of demineralized water): 7.5 g U-$^{13}C_6$ Glucose, 0.355 g 1,2-$^{13}C_2$- PAA, 0.5 g $(NH_4)H_2PO_4$,1.0 g $(NH_4)_2SO_4$, 0.5 g KH_2PO_4, 0.5 g $MgSO_4{\cdot}7H_2O$, 2.0 mL trace elements.

Fed-batch medium (per kg of demineralized water): 50 g U-$^{13}C_6$ Glucose, 1.207 g 1,2-$^{13}C_2$-PAA, 0.5 g $(NH_4)H_2PO_4$, 1.0 g $(NH_4)_2SO_4$, 0.5 g KH_2PO_4, 0.5 g $MgSO_4{\cdot}7H_2O$, 2.0 mL trace elements.

The trace element solution contained (per kg of demineralized water): 75 g $Na_2EDTA{\cdot}2H_2O$, 10 g $ZnSO_4{\cdot}7H_2O$, 10 g $MnSO_4{\cdot}1H_2O$, 20 g $FeSO_4{\cdot}7H_2O$, 2.5 g $CaCl_2{\cdot}2H_2O$, 2.5 g $CuSO_4{\cdot}5H_2O$.

For both the batch and fed-batch medium, the PAA was put in 100 mL demi-water and approximately 1/10 diluted ammonia solution was used to neutralize PAA until pH 6.0. Then the other compounds were added and dissolved. Subsequently the pH was adjusted to 6.5 with the same diluted ammonia solution.

2.1.4. Batch and fed-batch cultivation

Aerobic batch cultures (pH 6.5, 25 °C) of 0.3 L working volume were carried out in a 1 L turbine stirred bioreactor (Shanghai Guoqiang Bioengineering Equipment Co., Ltd, China). The batch cultivation was started with the inoculation of spore suspension from 1 g rice grains. The batch phase took about 12 h. When the DO and pH started to increase and the offgas CO_2 started to drop, the fed-batch phase was immediately started. The exponential feeding was controlled by the software to allow a specific biomass growth rate of 0.03 h^{-1}. The stirrer speed was primarily set at 150 RPM, gas flow rate, 0.3 L/min (1 vvm), oxygen saturation was set at 150% under an overpressure of 0.5 bar. The stirrer speed and gas flow rate were increased step-wise to 650 RPM and 0.6 L/min, respectively, whenever dissolved oxygen (DO)

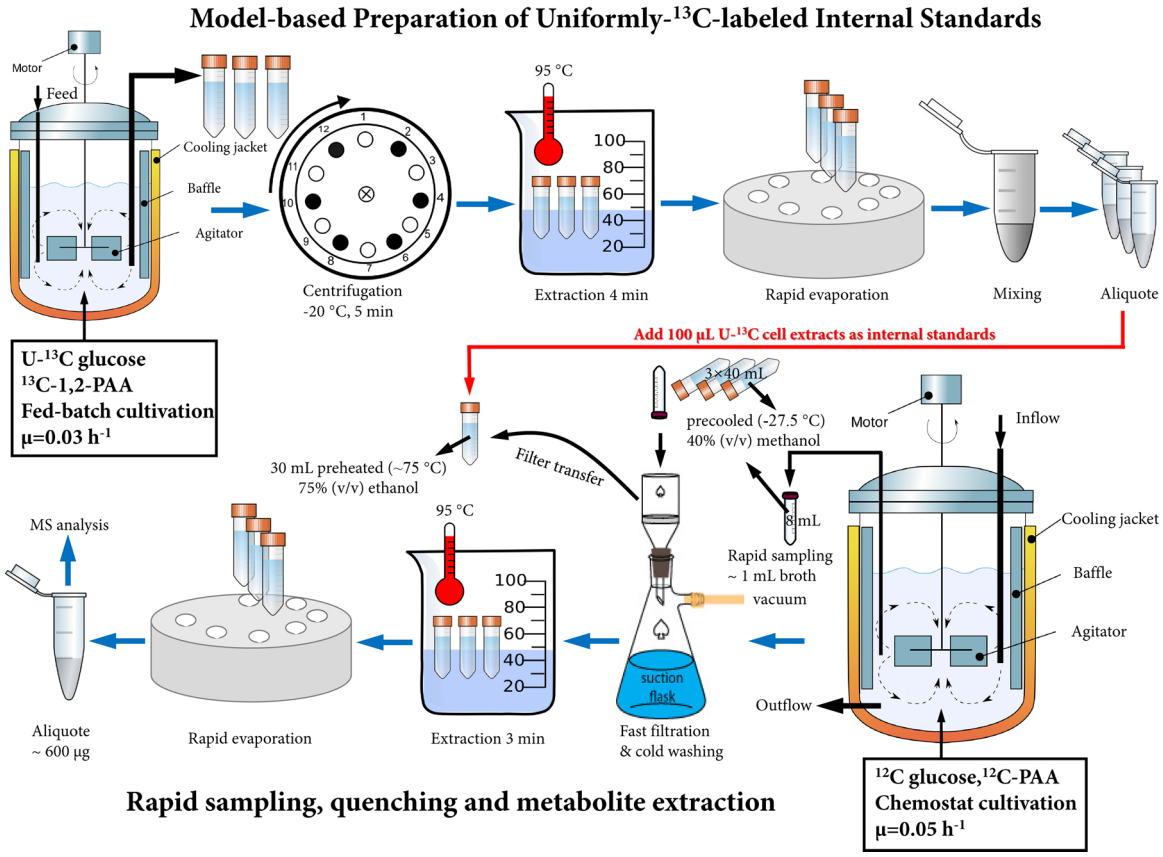

Fig. 1. Preparation of uniformly ^{13}C labeled cell extracts as internal standards, and the flowchart of well-established fast sampling, quenching and metabolite extraction procedure under quantitative metabolomics study of *P. chrysogenum*.

dropped close to 60%. It should be noted that removing unlabeled CO_2 from the air supply was accomplished by connecting a bottle of 4 M NaOH solution to the gas supply pipe before the air went into the bioreactor.

2.1.5. Rapid sampling, quenching and metabolite extraction

The fed-batch contained four phases. Phase I took about 47 h, and the first batch of 120 mL broth was rapidly taken into a beaker containing 500 mL 60% (v/v) methanol precooled at −80 °C. Then the mixture of broth and quenching solution was transferred to conical tubes, which were centrifuged at 4600 RPM for 5 min. Metabolite extraction was carried out immediately after the centrifugation. 30 mL pre-heated 75% (v/v) ethanol was transferred to each tube containing cell cakes, which were then put in 95 °C hot water bath for 4 min. After the extraction, the supernatant was collected by centrifugation. At the same time, the actual sampling weight was obtained by weighing the beaker before and after the sampling. The fraction of the sampled weight can be calculated, which should be multiplied by the current *FeedFactor* giving a new *FeedFactor*. This ensured that the remaining broth continued the exponential growth at the same growth rate of 0.03 h^{-1}. From this time on, every 1.5 h, the next Phases II and III were sampled. In Phase IV, a concentrated glucose pulse (about 2 ml of feed medium) was added to the remaining fed-batch broth. After about 1 min, the remaining broth was quenched and processed analogous to which was described above. Eventually, each tube containing the cell extract/ethanol solution was cooled on ice and subsequently concentrated in a Rapid-Vap (Labconco, Kansas City, MO) under controlled vacuum and room temperature to reach a final volume of approximately 5 mL. The concentrated cell extracts from all batches were fully mixed, 50 μL of which was taken to analysis to determine how much

Table 1
Parameters used in the kinetics of the metabolic model.

No.	Parameter	Value	Unit	Reference
1	Y_{SX}^{Max}	0.663	Cmol biomass/ Cmol glucose	van Gulik et al. (2001)
2	Y_{SP}^{Max}	0.029	mol penicillin/Cmol biomass	van Gulik et al. (2001)
3	m_S	0.0088	Cmol glucose/Cmol biomass/h	van Gulik et al. (2001)
4	q_S^{Max}	0.286	Cmol glucose/Cmol/h	de Jonge et al. (2011)
5	K_S	$4.68e^{-5}$	Cmol glucose/kg broth	de Jonge et al. (2011)
6	β	0.8	mol penicillin/Cmol biomass/h	Douma et al. (2010a, 2010b)
7	m	2	–	Douma et al. (2010a, 2010b)
8	k_{dE}	0.0147	1/h	Douma et al. (2010a, 2010b)
9	K_P	$6.5\ e^{-6}$	Cmol glucose/kg broth	This study
10	MW_{O2}	0.032	kg/molO_2	Douma et al. (2010a, 2010b)
11	MW_{CO2}	0.044	kg/molCO_2	Douma et al. (2010a, 2010b)
12	μ	0.03	1/h	This study

volume should be added to the samples in the metabolomics study. In general, the ratio of $^{12}C/^{13}C$ peak area determined by mass spectrometry in the experimental samples should be within an order of magnitude. The cell extracts were stored in −80 °C pending further use.

2.2. Part II. A case study with Penicillium chrysogenum for quantitative metabolomics study

2.2.1. Strain and medium

The same *Penicillium chrysogenum* DS 17,690 strain was used for all cultivations. The composition of batch and chemostat medium has been described previously (van Gulik et al., 2000). The minimal medium contained: (per kg of demineralized water): 16.5 g glucose monohydrate, 3.5 g $(NH_4)_2SO_4$, 0.8 g KH_2PO_4, 0.5 g $MgSO_4{\cdot}7H_2O$, 2 ml of a trace element solution. The trace element solution contained: (per kg of demineralized water) 75 g $Na_2EDTA{\cdot}2H_2O$, 10 g $ZnSO_4{\cdot}7H_2O$, 10 g $MnSO_4{\cdot}1H_2O$, 20 g $FeSO_4{\cdot}7H_2O$, 2.5 g $CaCl_2{\cdot}2H_2O$, 2.5 g $CuSO_4{\cdot}5H_2O$. The preparation and sterilization of the cultivation medium as well as the inoculation procedure have been described previously (Douma et al., 2010b).

2.2.2. Bioreactor cultivation

Aerobic glucose-limited chemostat cultures (pH 6.5, 25 °C, 2 L/min, 400 RPM) of 3 L working volume were carried out in a 5 L turbine stirred bioreactor (Shanghai Guoqiang Bioengineering Equipment Co., Ltd, China). All chemostat cultivations were operated at the dilution rate of 0.05 h^{-1} for 5 residence times (100 h) followed by rapid sampling under dynamic feeding strategies. In the present study, the dynamic feeding schemes were used for physiological characterization of the high-yielding *Penicillium chrysogenum* DS17690 strain. Experimental designs were as follows:

2.2.2.1. Design I single pulse response experiments. In this system, after 100 h of chemostat cultivation at the dilution rate of 0.05 h^{-1}, the pump speed was abruptly increased by a factor 10 for 36 s and switching it off for the following 324 s. Rapid sampling of broth for measurement of intracellular metabolites was carried out at 0, 5, 10, 20, 30, 35, 40, 50, 70, 90, 120, 150, 180, 210, 240, 270, 300, 330 and 360 s after the increase of the pump speed.

2.2.2.2. Design II repetitive glucose pulses. In this system before glucose in the batch medium was depleted, an intermittent feeding regime was imposed on the culture through the cultivation. An on/off feeding was applied with a cycle time of 3 min and 6 min, where the feed period was always 10% of the total on/off cycle. During the feeding interval, the pump speed was set 10 times higher than that under reference conditions to keep the average glucose feeding rate of the intermittently fed cultures the same as that of the control chemostats. The feed pump was precisely controlled by a timer, switching it on every first 36 s of the cycle for cycle times of 6 min, respectively. Rapid sampling of broth for measurement of intracellular metabolites was carried out after 100 h of intermittent feeding at 0, 8, 16, 26, 36, 50, 70, 90, 110, 145, 180, 200, 220, 240, 260, 280, 320 and 350 s within a complete 6 min feeding cycle.

2.2.3. Cell dry weight

An amount of 15 mL broth was withdrawn and split in triplicate for measurement of cell dry weight (CDW), using glass fiber filters (type A/E; Pall Corporation, East Hills, NY; 47 mm in diameter, 1-μm pore size), pre-dried overnight at 70 °C. For a CDW sample, 5 mL broth was filtered, and the cell cake was washed twice with 10 mL demineralized water and dried at 70 °C for 24 h. The biomass-containing filters were cooled to room temperature in a desiccator before weighing.

2.2.4. Rapid sampling, quenching and subsequent extraction for analysis of intracellular metabolites

To obtain snapshots of intracellular metabolites, samples were obtained within half a second by rapidly withdrawing about 1 mL of broth from the bioreactor, using a custom-made rapid sampling device, into a tube containing 8 mL 40% (v/v) methanol/water mixture at -27.5 °C for instantaneous quenching of the cell metabolism (de Jonge et al., 2012). The exact sample weights were determined by weighing all tubes before and after sampling. Fast filtration and a modified cold washing method were used for rapid and effective removal of all compounds present outside the cells (Douma et al., 2010a). The boiling ethanol method was adopted for rapid and reliable extraction of intracellular metabolites (Gonzalez et al., 1997). Prior to being exposed to the boiling solution, 24 μL of NEM and 120 μL of IS were added to the sample. According to the method, 30 mL of 75% (v/v) ethanol/water mixture (pre-heated at 75 °C) was then transferred to the cell pellet, followed by resuspension of the pellet and the sample tube was incubated in a 95 °C water bath for 3 min. Afterwards, the cell extract/ethanol solution was cooled on ice and subsequently concentrated in a Rapid-Vap (Labconco, Kansas City, MO) under controlled vacuum and room temperature to reach a final volume of approximately 300 μL. Before mass spectrometry-based analysis, the concentrated cell extracts were quantitated to 600 mg by adding Milli-Q water and filtered with a Millex HV 0.22 μm filter (Millipore, Billerica, MA) to remove cell debris. The filtrate was then stored at −80 °C pending further analysis.

2.2.5. Analytical procedures

Samples for metabolites quantification were analyzed using GC–MS (7890 A GC coupled to 5975C MSD, Agilent, Santa Clara, CA, USA) and LC–MS/MS (DIONEX Ultimate 3000 UPLC system coupled to a TSQ QUANTUM ULTRA mass spectrometer, Thermo Scientific, San Jose, USA). Metabolites of the glycolytic pathway, the TCA cycle and the PP pathway were quantified by GC–MS using the isotope dilution mass spectrometry (IDMS) method, as described previously (Cipollina et al., 2009; de Jonge et al., 2011; Wu et al., 2005). The concentrations of the nucleotides were also analyzed with the IDMS method; details of the applied LC–ESI–MS/MS procedure have been described elsewhere (Seifar et al., 2009).

3. Results and discussion

3.1. Production of U-^{13}C-labeled cell extracts

Unlike other primary metabolites, penicillin is a secondary metabolite and its pathway can only be fully induced at a very low growth rate, typically $\mu = 0.015\ h^{-1}$ has been used on an industrial-scale production. In most cases, the biomass specific growth rate is controlled by limited supply of the substrate, whereby glucose is frequently used. In order to obtain fully U-^{13}C-labeled biomass, *Penicillium chrysogenum* was grown on fully U-^{13}C-labeled glucose in an aerobic fed-batch culture, which was preceded by a batch phase. A previous study has shown that the highest penicillin productivity can be achieved at a growth rate of 0.03 h^{-1} under glucose-limited conditions (van Gulik et al., 2000). In order to obtain enough U-^{13}C-labeled metabolites from the penicillin biosynthetic pathway, *Penicillium chrysogenum* was therefore cultivated in a fed-batch mode where medium was exponentially fed to maintain the growth rate at 0.03 h^{-1}.

The fed-batch medium compositions, such as carbon source, nitrogen source and sulfur source, are critical to run a successful fed-batch fermentation. Important is to compute the consumption rate of each element. Then, based on these rates, the required concentrations of medium components can be estimated. In our preparation protocol, the feeding strategy was designed based on a previous published dynamic fed-batch model (Douma et al., 2010b). This model can

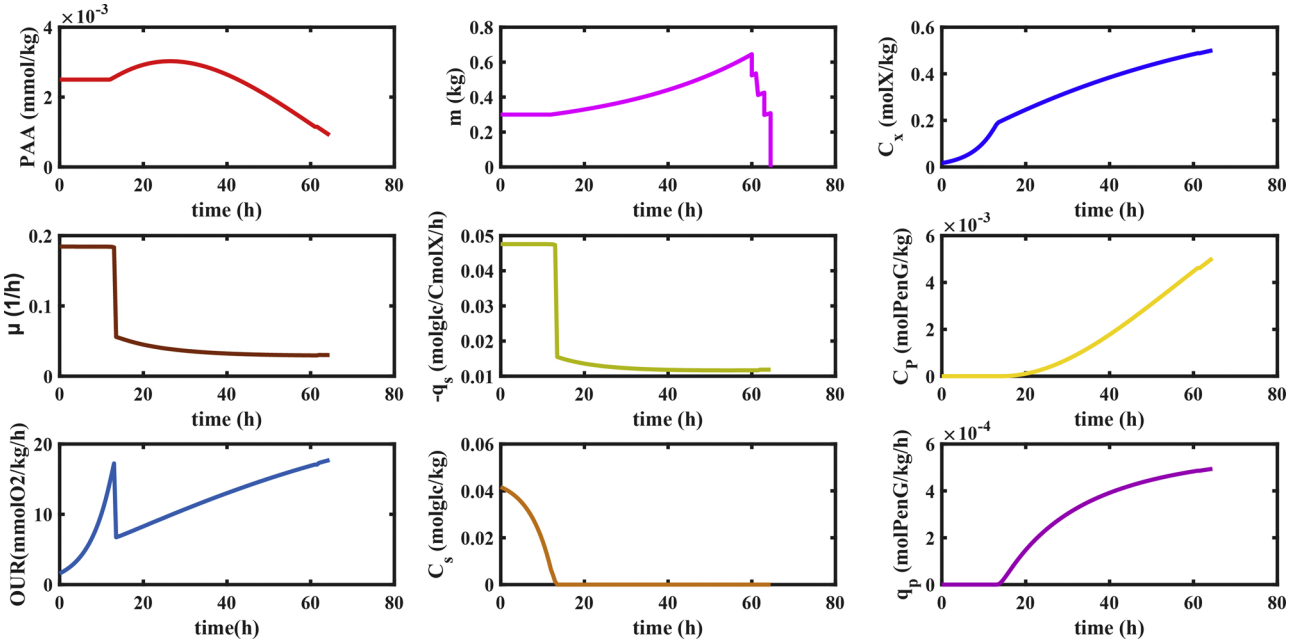

Fig. 2. Fed-batch process simulation using the dynamic fed-batch model.

accurately describe the biomass and penicillin concentrations for both chemostat steady-state as well as the dynamics during chemostat start-up and fed-batch cultivation. As shown in Fig. 2, process parameters such as concentrations of PAA, PenG, biomass as well as the relevant specific rates are predicted.

The whole fed-batch phase contained four sampling phases, i.e., 3 balanced state samplings and 1 perturbation-based sampling. In order to increase the levels of metabolites in the glycolysis, pentose phosphate pathway, tricarboxylic acid cycle, and energy metabolism, in Phase IV, a concentrated glucose pulse (about 2 ml of feed medium) was imposed on the remaining fed-batch broth. Quantitative results from liquid chromatography tandem mass spectrometry (LC–MS/MS) and gas chromatography tandem mass spectrometry (GC–MS) showed that concentrations of organic acids, sugar phosphates, amino acids and nucleotides were 2–10 folds higher than those without glucose pulse (data not shown). Eventually, extraction of the cultivated U-^{13}Clabeled biomass yielded essentially the whole *P. chrysogenum* metabolome and in principle, provided U-^{13}C-labeled internal standards for each intracellular metabolite of interest.

3.2. Calibration with labeled cell extract as internal standards (IS)

The standard ^{12}C samples for the calibration curves were prepared by diluting primary stock solutions of unlabeled metabolites with Milli-Q water to obtain 12 concentration levels (0.05, 0.1, 0.2, 0.5, 1, 2, 5, 10, 20, 50, 100 and 200 μM). Then, a fixed amount of 20% (v/v) ^{13}C-labeled cell extract was added to each calibration sample. The U-^{13}C-labeled extract of *P. chrysogenum* was prepared as described above.

The peak areas of the U-^{13}C and ^{12}C metabolites were measured either by GC–MS or LC–MS/MS according to the protocol described above. Linear calibration lines were obtained when the area ratios between the U-^{13}C and ^{12}C metabolites were plotted against the known concentrations of ^{12}C metabolites in the calibration standard. Table 2a–d shows the linearity of the IS-based calibration lines for different categorized metabolites. The calculated coefficients of determination (R^2) for all metabolites analyzed were very close to 1, which further substantiated the reliability of the isotope dilution method.

3.3. A case study: Adaptation of Penicillium chrysogenum during single and repetitive glucose perturbations

Nasution et al. (2006) carried out a first aerobic glucose-limited chemostat (D = 0.05 h^{-1}) study of the in vivo kinetic properties of primary metabolism (steady state and single pulse) of the same *Penicillium chrysogenum* strain. In Nasution's experiment, for the single glucose pulse carried out in the chemostat 16 ml of a 125 g/L glucose solution was injected into the reactor within 1 s. This increased the residual glucose concentration to approximately 0.5 g/L. Comparing the dynamics of the intracellular metabolites with similar glucose pulses, which resulted in an initial bulk glucose concentration of 0.5 g/L, imposed on chemostat cultures of *E. coli* (Taymaz-Nikerel et al., 2011) and *S. cerevisiae* (Mashego et al., 2006; Wu et al., 2006), revealed similar trends with respect to the intracellular metabolites: a) rapid increase of phosphorylated C_6 metabolites, b) rapid decrease in 2PG + 3PG and PEP, moderate increase in the TCA cycle intermediates and c) rapid achievement of a new pseudo-steady-state. However, there are also differences in the glucose pulse response among different microorganisms. For example, in *S. cerevisiae* (Mashego et al., 2006; Wu et al., 2006), ethanol was excreted as an overflow metabolite; no organic acids (e.g., citric, lactic, succinic, acetic acid) were excreted in the broth, but in Design I, an increase of intracellular storage carbohydrates was observed for *P. chrysogenum* (Fig. 3). This is consistent with one previous work (de Jonge et al., 2014). Neither of these phenomena (overflow or storage turnover) was observed in *E. coli* following a similar glucose pulse (Taymaz-Nikerel et al., 2011). In addition, *P. chrysogenum* cultures require over 100 s to attain a new metabolic steady state, much longer than the 30˜60 s needed for *E. coli* (Taymaz-Nikerel et al., 2013, 2011) and *S. cerevisiae* (Mashego et al., 2006; Visser et al., 2004). An explanation for the observed differences might be the difference in the q_s values. Because the increase of the glucose uptake rate induced by the glucose pulse is significantly higher in *E. coli* and *S. cerevisiae*, the rate of ATP regeneration is also higher. This would lead to the observed faster recovery of the new metabolic steady state compared to *P. chrysogenum*.

In the present study, Design I was also conducted, not only for comparison to earlier experiments, but especially for direct comparison with the repetitive glucose pulse experiments. Dynamics of intracellular metabolites (amino acids, sugar phosphates, organic acids and sugar

Table 2
Standard curves for amino acids, sugar phosphates, sugar alcohols, nucleotides and PenG pathway metabolites. X: the concentrations of known ^{12}C metabolites; Y: the peak areas ratio of ^{12}C and U-^{13}C-labeled metabolites.

(a) Standard curves for amino acids.

Compound	M/Z (^{12}C)	M/Z (^{13}C)	Standard curve	R^2
Alanine	260.1	263.1	Y = 0.0025X + 0.0028	0.996
Glycine	246.1	248.1	Y = 0.0203X + 0.1163	0.998
Valine	288.1	293.1	Y = 0.0325X + 0.1030	0.994
Leucine	274.1	279.1	Y = 0.1111X + 0.4382	0.992
Iso-leucine	274.1	279.1	Y = 0.1646X + 0.5650	0.992
Phenylalanine	336.2	345.2	Y = 0.4083X + 1.1821	0.994
Aspartate	418.2	422.2	Y = 0.0072X + 0.0267	0.995
Cysteine	406.1	409.1	Y = 0.0312X + 0.0979	0.999
Glutamate	474.3	479.3	Y = 0.0012X + 0.0076	0.994
Ornithine	184.1	188.1	Y = 0.0305X + 0.1668	0.983
Asparagine	417.2	421.2	Y = 0.0202X + 0.1104	0.990
α-aminoadipic acid	446.3	452.3	Y = 0.0625X + 0.2385	0.995
Lysine	431.3	437.3	Y = 0.0880X-0.0210	0.998
Glutamine	431.2	436.3	Y = 0.0019X + 0.0068	0.995
Histidine	440.3	446.3	Y = 0.0307X + 1.0542	0.990
Tyrosine	466.3	475.3	Y = 0.2657X + 0.0860	0.993
Tryptophan	375.2	386.2	Y = 0.5851X + 0.0446	0.970

(b) Standard curves for sugar phosphates, organic acids and sugar alcohols.

Compound	M/Z (^{12}C)	M/Z (^{13}C)	Standard curve	R^2
G6P	471.2	475.2	Y = 0.0230X + 0.0775	0.996
F6P	459.2	462.2	Y = 0.0601X + 0.1425	0.993
FBP	459.2	462.2	Y = 3.4206X-0.0114	0.999
2PG	459.1	462.1	Y = 3.6813X-0.0905	0.981
3PG	459.1	462.1	Y = 0.0209X + 0.0757	0.999
M1P	471.2	475.2	Y = 0.0234X + 0.0746	0.999
M6P	471.2	475.2	Y = 0.0534X + 0.1053	0.998
6PG	333.1	337.1	Y = 0.1626X-0.0227	0.768
R5P	315.2	317.2	Y = 0.0271X + 2.2617	0.948
Ribu5P	357.1	359.1	Y = 0.1592X + 0.0311	0.999
S7P	471.2	475.2	Y = 0.1280X + 0.0523	0.999
PEP	369.1	372.1	Y = 0.3731X + 0.6659	0.998
αKG	304.1	309.1	Y = 0.0985X + 0.0147	0.999
Citrate	465.2	471.2	Y = 0.0614X-0.2103	0.995
Iso-citrate	245.1	248.1	Y = 0.9894X-0.6987	0.992
Succinate	247.1	251.1	Y = 0.1195X + 0.2028	0.999
Fumarate	245.1	249.1	Y = 0.0613X + 0.1499	0.999
Malate	335.1	339.1	Y = 0.0199X + 0.0075	0.999
Trehalose	361.1	367.1	Y = 0.0014X + 0.0113	0.996
Erythritol	320.2	324.2	Y = 0.0013X + 0.0161	0.996
Mannitol	319.1	323.1	Y = 0.0002X + 0.0034	0.999
Arabitol	319.1	323.1	Y = 0.0028X + 0.0415	0.999
Glucose	319.1	323.1	Y = 0.0090X + 0.0061	0.999

(c) Standard curves for adenine nucleotides.

Compound	M/Z (^{12}C)	M/Z (^{13}C)	Standard curve	R^2
AMP	346.08	356.08	Y = 0.2448X + 0.1644	0.999
ADP	426.119	436.119	Y = 0.0557X + 0.0696	0.999
ATP	506.105	516.105	Y = 0.0167X + 0.0135	0.999

(d) Standard curves for penicillin pathway metabolites.

Compound	M/Z (^{12}C)	M/Z (^{13}C)	Standard curve	R^2
PAA	135.078	137.078	Y = 0.0014X + 0.0143	0.998
OPC	142.13	148.13	Y = 0.0038X + 0.0179	0.999
o-OH-PAA	151.069	153.069	Y = 0.0068X + 0.0345	0.999
6APA	215.112	223.112	Y = 0.0072X + 0.0488	0.997
PenG	333.098	343.098	Y = 0.0016X + 0.0095	0.998
PIO	351.151	361.151	Y = 0.0479X + 0.01601	0.999

alcohols) show largely different dynamic patterns upon a single glucose pulse and repetitive glucose pulses (Fig. 3). Applying a single glucose pulse results in a monotonous increase of most intracellular metabolites, while repetitive glucose pulses lead to the rhythmic patterns of the intracellular metabolites following the dynamics of the extracellular glucose and intracellular glucose-6-phosphate levels. Although the glucose peak concentrations after the single and repeated pulses likely were the same, the uptake of glucose after the peak apparently was different. After the single pulse the glucose uptake rate was slower such that during the full measurement period the glucose was not depleted,

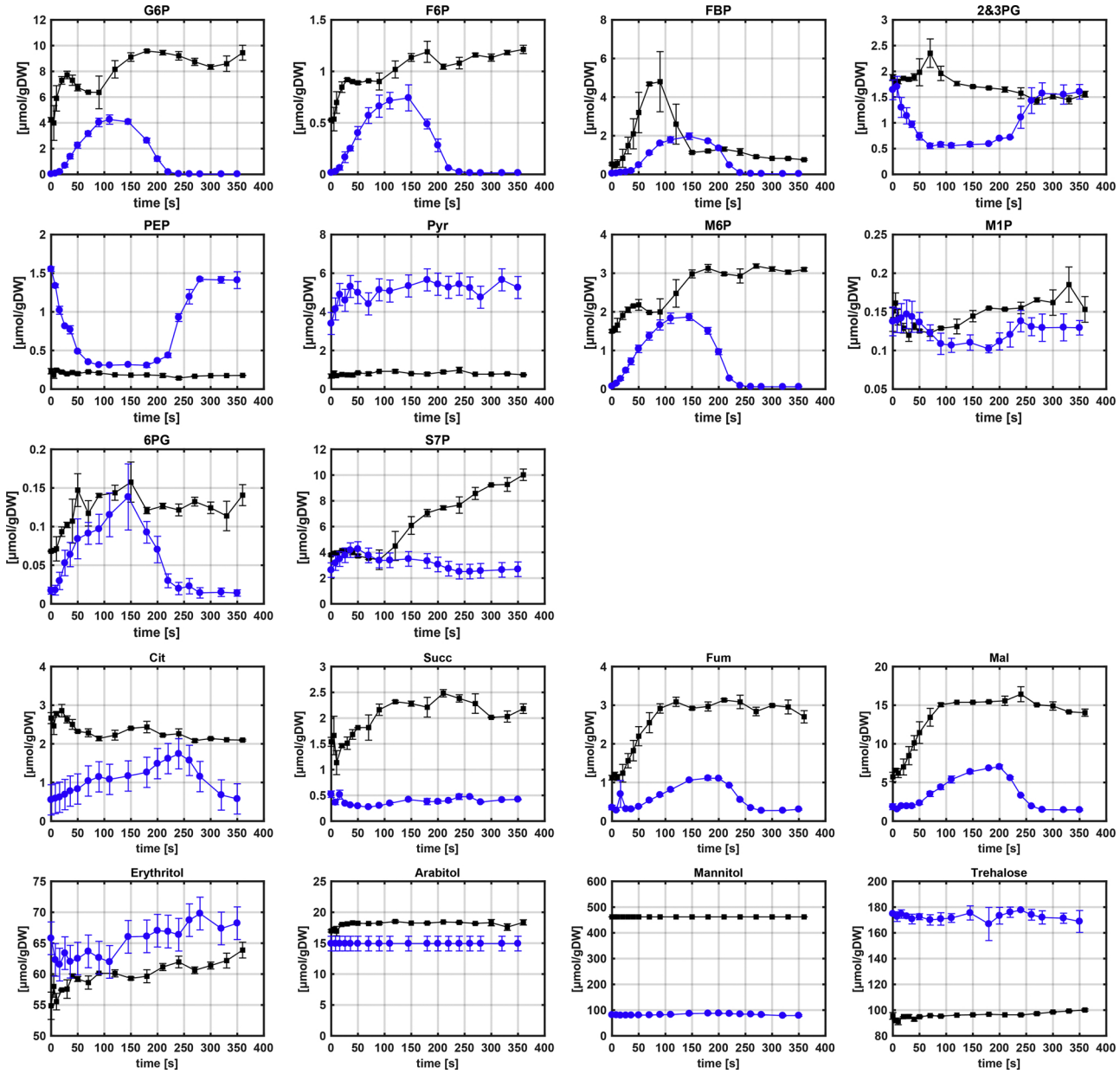

Fig. 3. a Measured amounts of intracellular sugar phosphates, organic acids and sugar alcohols) under single glucose (■) and repetitive glucose pulses (●). Fig.3b Measured amounts of intracellular amino acids under single glucose (■) and repetitive glucose pulses (●). Error bars represent standard deviation of three biological replicates.

while in the intermittent feeding the glucose uptake was faster such that starvation set in halfway the cycle.

Comparing single and repetitive 6 min pulse experiments, both the initial values and the dynamic profiles of amino acids (AAs), central metabolism and storage carbohydrates differed (Fig. 4). Interestingly, it was observed that in the 6 min repetitive glucose pulse case, these intracellular pool sizes (µmolC/gDW) were lower resulting in decreased turnover times, which was manifested by respectively 26%, 5% and 20% lower, intracellular pool sizes of amino acids, central carbon metabolism and storage carbohydrate. Particularly, the smaller storage carbohydrate pool might present a metabolic advantage because maintaining high levels of intracellular storage materials and overcapacity of pathway enzymes might be a metabolic burden (Mashego et al., 2005). However, accumulating evidence showed that storage turnover (e.g. trehalose storage and mobilization) is increased under dynamic cultivation conditions (de Jonge et al., 2014) and plays an indispensable role in maintaining cellular homeostasis, e.g. the inorganic phosphate balance (van Heerden et al., 2014). Consistent with this previous research, the intracellular amount of trehalose was about 2 times higher in repetitive glucose pulses (˜170 µmol/gDW) than in undisturbed chemostat cultures (˜95 µmol/gDW) in the current study. Upon a sudden glucose pulse (Design I), the pool size of amino acids rapidly increased by 47 µCmol/gDW within the first 30 s (5640 µCmol/gDCW/h), and then decreased by 69 µmolC/gDW within the following 330 s (753 µCmol/gDW/h). It has been previously reported that *P. chrysogenum* contains about 45% (w/w) protein (Henriksen et al., 1996). If the reduction of the pool of amino acids would be merely caused by biomass growth, then specific biomass growth rate (µ) would be 0.047 h^{-1}, which is very close to the cycle-average dilution rate of 0.05 h^{-1}. This suggests that under Design I after the pulse, *P. chrysogenum* started to fine-tune the µ based on the availability of pools of amino acids to avoid too much overshoot of µ. This might be related

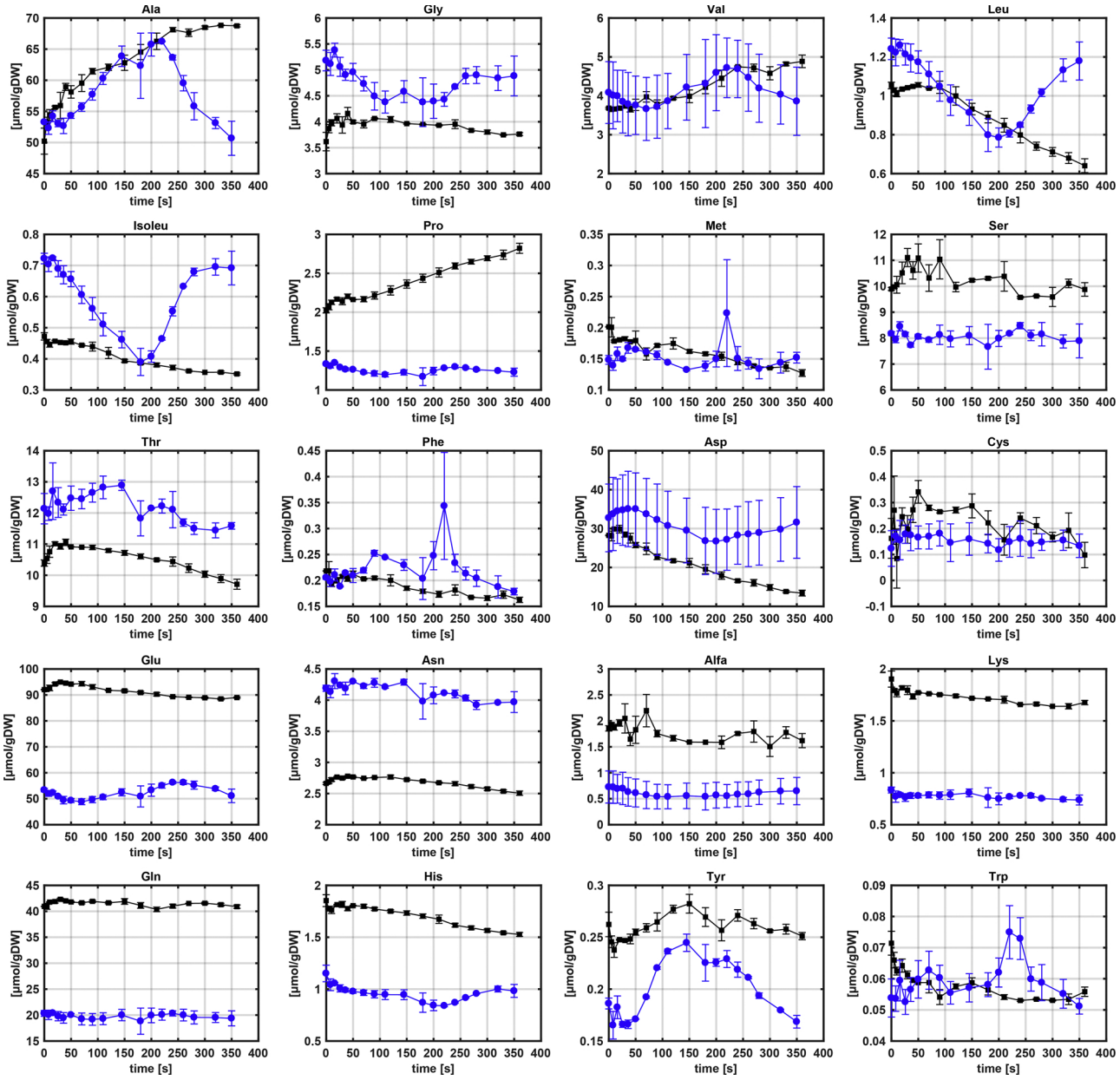

Fig. 3. (*continued*)

with the decreasing extracellular glucose concentrations, as it may be sensed by glucosensing proteins on the filaments of *P. chrysogenum* (Wang et al., 2018a). Within the first 30 s of medium feeding, the total carbon in the metabolites (amino acids, central carbon metabolites and storage carbohydrates) was increased by 1858 ± 61 µmolC, irrespective of the growth dilution, which is equivalent to a biomass specific glucose uptake rate of 0.0604 ± 0.002 mol/CmolX/h. This value is 45% higher than the q_s^{max} = 0.0417 mol/CmolX/h used in the 6 min repetitive glucose pulses (Tang et al., 2017; Wang et al., 2018b), but still in the range of estimated q_s^{max} and uptake capacity as reported by de Jonge et al. (2011) and Tang et al. (2017), respectively. This indicated that the average glucose uptake rate within the following 324 s after the pulse would be lower than 0.023 mol/CmolX/h which can be calculated provided all initial glucose would be consumed, which is, however, apparently not the case as can be inferred from the metabolite patterns (Fig. 3). The results also revealed that there is dynamic regulation of the glycolysis where glucose uptake and phosphorylation occur. The glucose uptake is rapidly inhibited when glycolytic intermediates accumulates to buffer temporary nutrient excess, and the stored intermediates can be re-consumed in over 6 min after the pulse. In addition, this repression of glucose uptake may be also caused by transient decrease of intracellular inorganic phosphate level (van Heerden et al., 2014).

Fig. 4 further shows the time patterns of the adenine nucleotide levels and the energy charge (EC). Upon an abrupt glucose perturbation, the intracellular ATP level decreases linearly from 0 to 70 s, which is accompanied by an increase of the levels of ADP and AMP. Subsequently, the ATP level remains 44% lower than that before the pulse in the following 5 min. In line with the ATP paradox phenomena as previously observed in *S. cerevisiae* (Aledo et al., 2008; Somsen et al., 2000), the summed level of the adenine nucleotide drops significantly after the sudden addition of the glucose (Fig. 4). It has been reported that the transient accumulation of the purine salvage pathway intermediate, inosine, accounted for the apparent loss of adenine nucleotides, and this interconversion facilitates rapid and energy-cost efficient adaptation of the AXP pool size to changing environmental conditions (Walther et al., 2010). In contrast, the repetitive glucose pulses do not show a sudden loss of the ATP pool size and the disruption of nucleotide

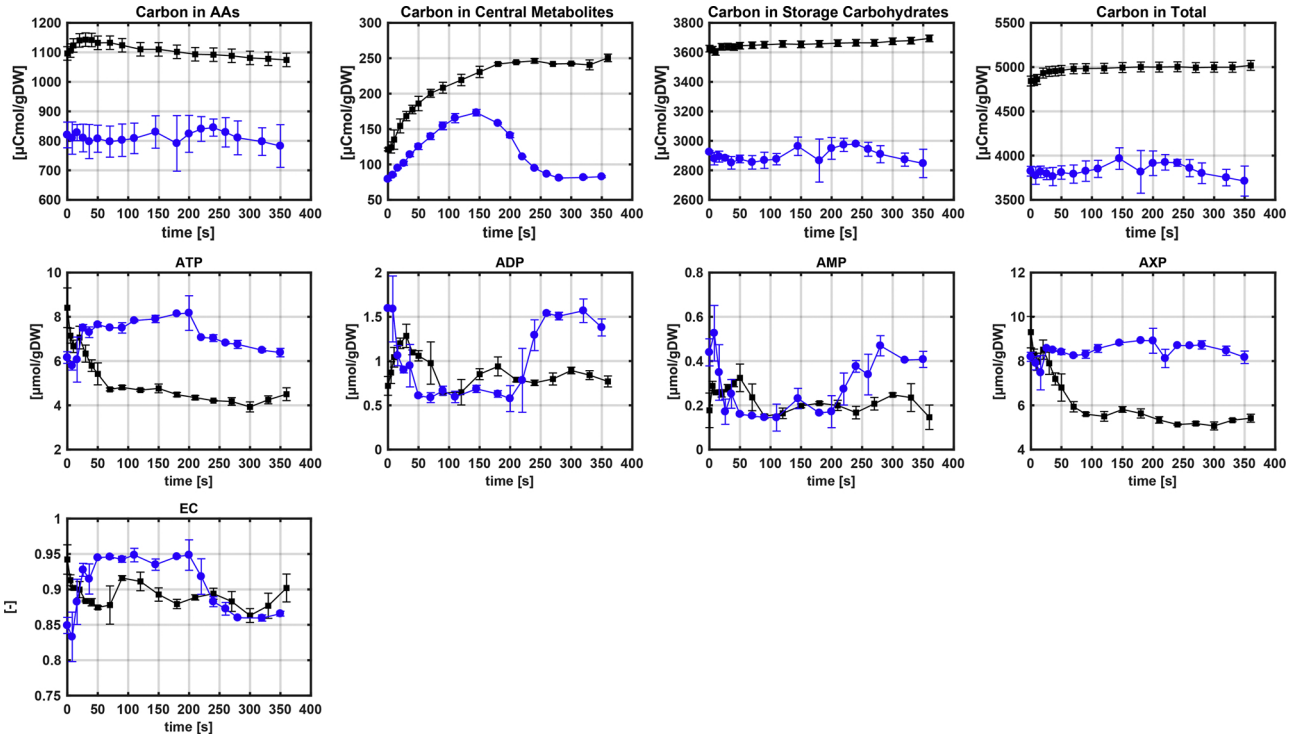

Fig. 4. Dynamics of intracellular carbon pools of amino acids (AAs), central metabolism, storage carbohydrate, and dynamic of intracellular adenine nucleotide levels and the energy charge under single glucose (■) and repetitive glucose pulses (●). Error bars represent standard deviation of three biological replicates.

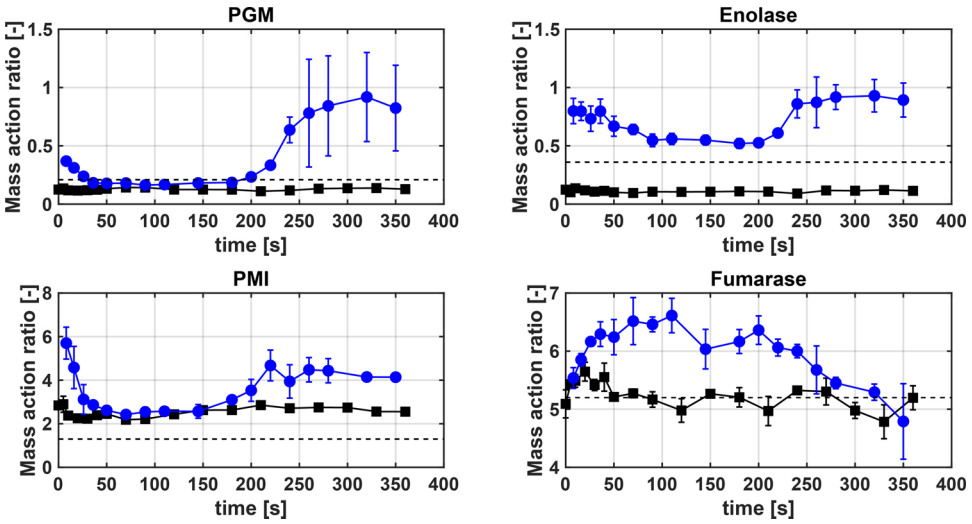

Fig. 5. Mass action ratios for phosphoglucose isomerase (PGI), enolase and fumarase under single glucose (■) and repetitive glucose pulses (●). The dash lines represent equilibrium values. Error bars represent standard deviation of three biological replicates.

homeostasis, e.g., the AXP pool size and the energy charge (Fig. 4), indicating that the cells have been readily 'trained' to actively cope with the periodic glucose perturbations. This highly coordinated metabolism can also be discernible by the changes in the intracellular metabolite concentrations (Fig. 3).

Consistent with significant differences in intracellular metabolite profiles following sudden and repetitive glucose perturbations, mass action ratios (MARs) for phosphoglucoisomerase (PGI), phosphomannose-isomerase (PMI), enolase and fumarase exhibit different dynamics (Fig. 5). Under 6 min repetitive glucose pulse conditions, these MARs are all increased above their equilibrium values in the glucose deprivation phase, showing that reversed flux occurs because central metabolites are consumed. This scenario can only occur when these central metabolites accumulate in the glucose abundant phase and then are re-consumed in the glucose deprivation phase (Wang et al., 2018b). This can be indeed observed in the intracellular metabolite concentrations (Fig. 3). However, following a single glucose pulse, these MARs remain closer to their equilibrium values. This suggests that upon a single glucose pulse, these reactions still operated close to equilibrium, i.e., without precise regulatory control at the metabolite level, posing a threat to maintaining a cellular balanced state. In contrast, under repetitive glucose pulses, cells were trained to cater for the fast substrate dynamics, and the toggles of these reactions were switched on to re-distribute the influx of the substrate and accelerate the utilization of the accumulated intermediates in the glucose deprivation phase.

4. Conclusions

The U-^{13}C cell extract from the *P. chrysogenum* strain was successfully prepared based on the simulation results by a dynamic fed-batch model. The obtained U-^{13}C cell extracts can be used for quantitative

metabolomics study of *P. chrysogenum* under both steady state and dynamic conditions. The case study showed that this *P. chrysogenum* strain dissimilarly responded to a sudden glucose pulse and repetitive glucose perturbations, in terms of metabolite concentration patterns in the time range of 360 s A typical difference was the response of the adenine nucleotides (ATP, ADP and AMP): the loss of the adenine nucleotide pool was observed following a sudden glucose pulse, but this pool remained unchanged in repetitive glucose perturbations. Further, under repetitive glucose perturbations, relieving the metabolic burden appears to be at a price of increased levels of lower glycolytic intermediates (Pyruvate, PEP) and storage carbohydrates (trehalose) and reduced influx of secondary pathways such as the PPP and the TCA cycle. In general, results from dynamic experiments with a single disturbance of the steady state might not be relevant for repetitive dynamics, like those governing in large-scale bioreactors or studied in scale-down simulators. This discrepancy suggests that *P. chrysogenum* would use different regulatory systems to respond to fast changing environments or perturbations. As a result, by using the IDMS method, quantitative time-resolved metabolite data can serve to the generation of hypotheses on molecular mechanisms and metabolic regulation under relevant scale-down conditions.

Conflict of interest

The authors declare there are no competing interest.

Acknowledgement

This work was financially subsidized by the NWO-MoST Joint Program, Grant number, 2013DFG32630, the 111 Project (B18022), the National key research and development program, 2017ZX7402003, and the Fundamental Research Funds for the Central Universities, 22221818014.

References

Aledo, J.C., Jimenez-Riverez, S., Cuesta-Munoz, A., Romero, J.M., 2008. The role of metabolic memory in the ATP paradox and energy homeostasis. FEBS J. 275, 5332–5342. https://doi.org/10.1111/j.1742-4658.2008.06663.x.

Almquist, J., Cvijovic, M., Hatzimanikatis, V., Nielsen, J., Jirstrand, M., 2014. Kinetic models in industrial biotechnology – improving cell factory performance. Metab. Eng. 24, 38–60. https://doi.org/10.1016/j.ymben.2014.03.007.

Bennett, B.D., Yuan, J., Kimball, E.H., Rabinowitz, J.D., 2008. Absolute quantitation of intracellular metabolite concentrations by an isotope ratio-based approach. Nat. Protoc. 3, 1299–1311. https://doi.org/10.1038/nprot.2008.107.

Canelas, A.B., Harrison, N., Fazio, A., Zhang, J., Pitkanen, J.P., van den Brink, J., Bakker, B.M., Bogner, L., Bouwman, J., Castrillo, J.I., Cankorur, A., Chumnanpuen, P., Daran-Lapujade, P., Dikicioglu, D., van Eunen, K., Ewald, J.C., Heijnen, J.J., Kirdar, B., Mattila, I., Mensonides, F.I., Niebel, A., Penttila, M., Pronk, J.T., Reuss, M., Salusjarvi, L., Sauer, U., Sherman, D., Siemann-Herzberg, M., Westerhoff, H., de Winde, J., Petranovic, D., Oliver, S.G., Workman, C.T., Zamboni, N., Nielsen, J., 2010. Integrated multilaboratory systems biology reveals differences in protein metabolism between two reference yeast strains. Nat. Commun. 1, 145. https://doi.org/10.1038/ncomms1150.

Chubukov, V., Uhr, M., Le Chat, L., Kleijn, R.J., Jules, M., Link, H., Aymerich, S., Stelling, J., Sauer, U., 2013. Transcriptional regulation is insufficient to explain substrate-induced flux changes in *Bacillus subtilis*. Mol. Syst. Biol. 9, 709. https://doi.org/10.1038/msb.2013.66.

Cipollina, C., ten Pierick, A., Canelas, A.B., Seifar, R.M., van Maris, A.J., van Dam, J.C., Heijnen, J.J., 2009. A comprehensive method for the quantification of the non-oxidative pentose phosphate pathway intermediates in *Saccharomyces cerevisiae* by GC-IDMS. J. Chromat. B, Analyt. Technol. Biomed. Life Sci. 877, 3231–3236. https://doi.org/10.1016/j.jchromb.2009.07.019.

de Jonge, L.P., Buijs, N.A., ten Pierick, A., Deshmukh, A., Zhao, Z., Kiel, J.A., Heijnen, J.J., van Gulik, W.M., 2011. Scale-down of penicillin production in *Penicillium chrysogenum*. Biotechnol. J. 6, 944–958. https://doi.org/10.1002/biot.201000409.

de Jonge, L.P., Douma, R.D., Heijnen, J.J., van Gulik, W.M., 2012. Optimization of cold methanol quenching for quantitative metabolomics of *Penicillium chrysogenum*. Metabolomics 8, 727–735. https://doi.org/10.1007/s11306-011-0367-3.

de Jonge, L.P., Buijs, N.A., Heijnen, J.J., van Gulik, W.M., Abate, A., Wahl, S.A., 2014. Flux response of glycolysis and storage metabolism during rapid feast/famine conditions in *Penicillium chrysogenum* using dynamic (13) C labeling. Biotechnol. J. 9, 372–385. https://doi.org/10.1002/biot.201200260.

Deshmukh, A.T., Verheijen, P.J., Seifar, R.M., Heijnen, J.J., van Gulik, W.M., 2015. In vivo kinetic analysis of the penicillin biosynthesis pathway using PAA stimulus response experiments. Metab. Eng. 32, 155–173. https://doi.org/10.1016/j.ymben.2015.09.018.

Douma, R.D., de Jonge, L.P., Jonker, C.T.H., Seifar, R.M., Heijnen, J.J., van Gulik, W.M., 2010a. Intracellular metabolite determination in the presence of extracellular abundance: application to the penicillin biosynthesis pathway in *Penicillium chrysogenum*. Biotechnol. Bioeng. 107, 105–115. https://doi.org/10.1002/bit.22786.

Douma, R.D., Verheijen, P.J., de Laat, W.T., Heijnen, J.J., van Gulik, W.M., 2010b. Dynamic gene expression regulation model for growth and penicillin production in *Penicillium chrysogenum*. Biotechnol. Bioeng. 106, 608–618. https://doi.org/10.1002/bit.22689.

Fiehn, O., 2002. Metabolomics–the link between genotypes and phenotypes. Plant Mol. Biol. 48, 155–171. https://doi.org/10.1007/978-94-010-0448-0_11.

Gerosa, L., Sauer, U., 2011. Regulation and control of metabolic fluxes in microbes. Curr. Opin. Biotechnol. 22, 566–575. https://doi.org/10.1016/j.copbio.2011.04.016.

Gonzalez, B., François, J., Renaud, M., 1997. A rapid and reliable method for metabolite extraction in yeast using boiling buffered ethanol. Yeast 13, 1347–1355. https://doi.org/10.1002/(SICI)1097-0061(199711)13:14<1347::AID-YEA176>3.0.CO;2-O.

Hackett, S.R., Zanotelli, V.R., Xu, W., Goya, J., Park, J.O., Perlman, D.H., Gibney, P.A., Botstein, D., Storey, J.D., Rabinowitz, J.D., 2016. Systems-level analysis of mechanisms regulating yeast metabolic flux. Science 354https://doi.org/10.1126/science.aaf2786. aaf2786.

Henriksen, C.M., Christensen, L.H., Nielsen, J., Villadsen, J., 1996. Growth energetics and metabolic fluxes in continuous cultures of *Penicillium chrysogenum*. J. Biotechnol. 45, 149–164. https://doi.org/10.1016/0168-1656(95)00164-6.

Li, C., Shu, W., Wang, S., Liu, P., Zhuang, Y., Zhang, S., Xia, J., 2018. Dynamic metabolic response of *Aspergillus niger* to glucose perturbation: evidence of regulatory mechanism for reduced glucoamylase production. J. Biotechnol. 287, 28–40. https://doi.org/10.1016/j.jbiotec.2018.08.005.

Link, H., Fuhrer, T., Gerosa, L., Zamboni, N., Sauer, U., 2015. Real-time metabolome profiling of the metabolic switch between starvation and growth. Nat Met 12, 1091–1097. https://doi.org/10.1038/nmeth.3584.

Mashego, M.R., Wu, L., Van Dam, J.C., Ras, C., Vinke, J.L., Van Winden, W.A., Van Gulik, W.M., Heijnen, J.J., 2004. MIRACLE: mass isotopomer ratio analysis of U-^{13}C-labeled extracts. A new method for accurate quantification of changes in concentrations of intracellular metabolites. Biotechnol. Bioeng. 85, 620–628. https://doi.org/10.1002/bit.10907.

Mashego, M.R., Jansen, M.L., Vinke, J.L., van Gulik, W.M., Heijnen, J.J., 2005. Changes in the metabolome of *Saccharomyces cerevisiae* associated with evolution in aerobic glucose-limited chemostats. FEMS Yeast Res. 5, 419–430. https://doi.org/10.1016/j.femsyr.2004.11.008.

Mashego, M.R., van Gulik, W.M., Vinke, J.L., Visser, D., Heijnen, J.J., 2006. In vivo kinetics with rapid perturbation experiments in *Saccharomyces cerevisiae* using a second-generation BioScope. Metab. Eng. 8, 370–383. https://doi.org/10.1016/j.ymben.2006.02.002.

Nasution, U., van Gulik, W.M., Proell, A., van Winden, W.A., Heijnen, J.J., 2006. Generating short-term kinetic responses of primary metabolism of *Penicillium chrysogenum* through glucose perturbation in the bioscope mini reactor. Metab. Eng. 8, 395–405. https://doi.org/10.1016/j.ymben.2006.04.002.

Nasution, U., van Gulik, W.M., Ras, C., Proell, A., Heijnen, J.J., 2008. A metabolome study of the steady-state relation between central metabolism, amino acid biosynthesis and penicillin production in *Penicillium chrysogenum*. Metab. Eng. 10, 10–23. https://doi.org/10.1016/j.ymben.2007.07.001.

Ozcengiz, G., Demain, A.L., 2013. Recent advances in the biosynthesis of penicillins, cephalosporins and clavams and its regulation. Biotechnol. Adv. 31, 287–311. https://doi.org/10.1016/j.biotechadv.2012.12.001.

Patacq, C., Chaudet, N., Letisse, F., 2018. Absolute quantification of ppGpp and pppGpp by double-spike isotope dilution ion chromatography-high-Resolution mass spectrometry. Anal. Chem. 90, 10715–10723. https://doi.org/10.1021/acs.analchem.8b00829.

Prausse, M.T., Schauble, S., Guthke, R., Schuster, S., 2016. Computing the various pathways of penicillin synthesis and their molar yields. Biotechnol. Bioeng. 113, 173–181. https://doi.org/10.1002/bit.25694.

Reznik, E., Christodoulou, D., Goldford, J.E., Briars, E., Sauer, U., Segre, D., Noor, E., 2017. Genome-scale architecture of small molecule regulatory networks and the fundamental trade-off between regulation and enzymatic activity. Cell Rep. 20, 2666–2677. https://doi.org/10.1016/j.celrep.2017.08.066.

Schatschneider, S., Abdelrazig, S., Safo, L., Henstra, A.M., Millat, T., Kim, D.H., Winzer, K., Minton, N.P., Barrett, D.A., 2018. Quantitative isotope-dilution high-resolution-Mass-Spectrometry analysis of multiple intracellular metabolites in *Clostridium autoethanogenum* with uniformly (13)C-Labeled standards derived from Spirulina. Anal. Chem. 90, 4470–4477. https://doi.org/10.1021/acs.analchem.7b04758.

Seifar, R.M., Zhao, Z., van Dam, J., van Winden, W., van Gulik, W., Heijnen, J.J., 2008. Quantitative analysis of metabolites in complex biological samples using ion-pair reversed-phase liquid chromatography-isotope dilution tandem mass spectrometry. J. Chromatogr. A 1187, 103–110. https://doi.org/10.1016/j.chroma.2008.02.008.

Seifar, R.M., Ras, C., van Dam, J.C., van Gulik, W.M., Heijnen, J.J., van Winden, W.A., 2009. Simultaneous quantification of free nucleotides in complex biological samples using ion pair reversed phase liquid chromatography isotope dilution tandem mass spectrometry. Anal. Biochem. 388, 213–219. https://doi.org/10.1016/j.ab.2009.02.025.

Somsen, O.J., Hoeben, M.A., Esgalhado, E., Snoep, J.L., Visser, D., van der Heijden, R.T., Heijnen, J.J., Westerhoff, H.V., 2000. Glucose and the ATP paradox in yeast. Biochem. J. 352 (Pt 2), 593–599. https://doi.org/10.1042/bj3520593.

Stafsnes, M.H., Rost, L.M., Bruheim, P., 2018. Improved phosphometabolome profiling applying isotope dilution strategy and capillary ion chromatography-tandem mass spectrometry. J. Chromat. B, Analyt. Technol. Biomed. Life Sci. 1083, 278–283.

https://doi.org/10.1016/j.jchromb.2018.02.004.
Tang, W., Deshmukh, A.T., Haringa, C., Wang, G., van Gulik, W., van Winden, W., Reuss, M., Heijnen, J.J., Xia, J., Chu, J., Noorman, H.J., 2017. A 9-pool metabolic structured kinetic model describing days to seconds dynamics of growth and product formation by *Penicillium chrysogenum*. Biotechnol. Bioeng. 114, 1733–1743. https://doi.org/10.1002/bit.26294.
Taymaz-Nikerel, H., van Gulik, W.M., Heijnen, J.J., 2011. *Escherichia coli* responds with a rapid and large change in growth rate upon a shift from glucose-limited to glucose-excess conditions. Metab. Eng. 13, 307–318. https://doi.org/10.1016/j.ymben.2011.03.003.
Taymaz-Nikerel, H., De Mey, M., Baart, G., Maertens, J., Heijnen, J.J., van Gulik, W., 2013. Changes in substrate availability in *Escherichia coli* lead to rapid metabolite, flux and growth rate responses. Metab. Eng. 16, 115–129. https://doi.org/10.1016/j.ymben.2013.01.004.
van Gulik, W.M., de Laat, W.T., Vinke, J.L., Heijnen, J.J., 2000. Application of metabolic flux analysis for the identification of metabolic bottlenecks in the biosynthesis of penicillin-G. Biotechnol. Bioeng. 68, 602–618. https://doi.org/10.1002/(SICI)1097-0290(20000620)68:6<602::AID-BIT3>3.0.CO;2-2.
van Gulik, W.M., Antoniewicz, M.R., deLaat, W.T.A.M., Vinke, J.L., Heijnen, J.J., 2001. Energetics of growth and penicillin production in a high-producing strain of *Penicillium chrysogenum*. Biotechnol. Bioeng. 72, 185–193. https://doi.org/10.1002/1097-0290(20000120)72:2<185::AID-BIT7>3.0.CO;2-M.
van Heerden, J.H., Wortel, M.T., Bruggeman, F.J., Heijnen, J.J., Bollen, Y.J., Planque, R., Hulshof, J., O'Toole, T.G., Wahl, S.A., Teusink, B., 2014. Lost in transition: start-up of glycolysis yields subpopulations of nongrowing cells. Science 343https://doi.org/10.1126/science.1245114. 1245114.
Vielhauer, O., Zakhartsev, M., Horn, T., Takors, R., Reuss, M., 2011. Simplified absolute metabolite quantification by gas chromatography-isotope dilution mass spectrometry on the basis of commercially available source material. J. Chromat. B, Analyt. Technol. Biomed. Life Sci. 879, 3859–3870. https://doi.org/10.1016/j.jchromb.2011.10.036.
Visser, D., van Zuylen, G.A., van Dam, J.C., Eman, M.R., Proll, A., Ras, C., Wu, L., van Gulik, W.M., Heijnen, J.J., 2004. Analysis of in vivo kinetics of glycolysis in aerobic *Saccharomyces cerevisiae* by application of glucose and ethanol pulses. Biotechnol. Bioeng. 88, 157–167. https://doi.org/10.1002/bit.20235.
Walther, T., Novo, M., Rossger, K., Letisse, F., Loret, M.O., Portais, J.C., Francois, J.M., 2010. Control of ATP homeostasis during the respiro-fermentative transition in yeast. Mol. Syst. Biol. 6, 344. https://doi.org/10.1038/msb.2009.100.
Wang, G., Wu, B., Zhao, J., Haringa, C., Xia, J., Chu, J., Zhuang, Y., Zhang, S., Heijnen, J.J., van Gulik, W., Deshmukh, A.T., Noorman, H.J., 2018a. Power input effects on degeneration in prolonged penicillin chemostat cultures: a systems analysis at flux, residual glucose, metabolite, and transcript levels. Biotechnol. Bioeng. 115, 114–125. https://doi.org/10.1002/bit.26447.
Wang, G., Zhao, J., Haringa, C., Tang, W., Xia, J., Chu, J., Zhuang, Y., Zhang, S., Deshmukh, A.T., van Gulik, W., Heijnen, J.J., Noorman, H.J., 2018b. Comparative performance of different scale-down simulators of substrate gradients in *Penicillium chrysogenum* cultures: the need of a biological systems response analysis. Microb. Biotechnol. 11, 486–497. https://doi.org/10.1111/1751-7915.13046.
Wang, G., Zhao, J., Wang, X., Wang, T., Zhuang, Y., Chu, J., Zhang, S., Noorman, H.J., 2019. Quantitative metabolomics and metabolic flux analysis reveal impact of altered trehalose metabolism on metabolic phenotypes of *Penicillium chrysogenum* in aerobic glucose-limited chemostats. Biochem. Eng. J. 146, 41–51. https://doi.org/10.1016/j.bej.2019.03.006.
Wu, L., Mashego, M.R., van Dam, J.C., Proell, A.M., Vinke, J.L., Ras, C., van Winden, W.A., van Gulik, W.M., Heijnen, J.J., 2005. Quantitative analysis of the microbial metabolome by isotope dilution mass spectrometry using uniformly ^{13}C-labeled cell extracts as internal standards. Anal. Biochem. 336, 164–171. https://doi.org/10.1016/j.ab.2004.09.001.
Wu, L., van Dam, J., Schipper, D., Kresnowati, M.T., Proell, A.M., Ras, C., van Winden, W.A., van Gulik, W.M., Heijnen, J.J., 2006. Short-term metabolome dynamics and carbon, electron, and ATP balances in chemostat-grown *Saccharomyces cerevisiae* CEN.PK 113-7D following a glucose pulse. Appl. Environ. Microbiol. 72, 3566–3577. https://doi.org/10.1128/AEM.72.5.3566-3577.2006.